Energy Conversion and Management 105 (2015) 858–871

Contents lists available at ScienceDirect

Energy Conversion and Management

journal homepage: www.elsevier.com/locate/enconman

Exploring the limits of a down-sized ethanol direct injection spark ignited engine in different configurations in order to replace high-displacement gasoline engines

José Guilherme Coelho Baêta [a,*], Michael Pontoppidan [b], Thiago R.V. Silva [a]

[a] Centro de Tecnologia da Mobilidade, Universidade Federal de Minas Gerais (UFMG), Av. Presidente Antônio Carlos 6627, Belo Horizonte, MG, Brazil
[b] Numidis S.a.r.l., France

ARTICLE INFO

Article history:
Received 24 March 2015
Accepted 14 August 2015

Keywords:
Down-sizing
Ethanol direct injection
Turbocharged
Down-speeding
Exhaust Gas Recirculation

ABSTRACT

The paper presents a layout of a highly boosted Ethanol Direct Injected engine in order to explore the limits of down-sizing for replacing high-displacement gasoline engines, which represents a powerful means of reducing fuel consumption and engine-out emissions at reduced production costs. The substitution of high-displacement engines (2.4- or 3.0-l) by a down-sized turbocharged Ethanol Direct Injected engine is studied. This document describes the detailed layout of all engine hardware and in particular, the cylinder head structure including the optimized intake and exhaust manifolds as well as implemented direct injection injectors. The work continues with a presentation of the experimental data obtained at the engine test rig. A series of experimental data is also presented for the down-sized engine mounted in a car as a replacement for its original high-displacement engine. Substantial fuel consumption gains are obtained as well as values of engine torque for the down-sized, down-speeded prototype engine, which makes it possible to replace engines with much higher displacements. As a result the maximum obtained efficiency of the 1.4 l prototype engine with twin-stage compressor reaches a value of 3250 kPa brake pressure at 44% efficiency. The present work is a very new and different approach compared to previous published studies on ethanol and down-sized engines due to the fact that the Brazilian hydrated ethanol fuel (7% water content) has a major charge effect compared to North American and European Gasoline and alcohol fuels (consult Table 1). This means that more aggressive down-sizing, turbo-charging and mixture stratification approaches can be applied as the following chapters will explain in detail.

1. Introduction

The approach of combining highly boosted Ethanol Direct Injected (EDI) engines with extreme down-sizing represents a powerful means of reducing CO_2 emissions as well as reducing engine production costs. It makes it possible to replace high-displacement gasoline (E0) or flex fuel (E22) engines with smaller highly boosted engines running on bio-fuels such as hydrated ethanol in Brazil (E100) or in North America and Europe (E85). The denomination "Ex", where *x* can be a random number between 0 and 100 is currently used in the automotive terminology to indicate the fraction of ethanol blended into pure gasoline. Why use alcohol fuels? The oxidation within the combustion chamber of both a carbon and an alcohol-based fuel produces inevitably, amongst other pollutants, CO_2 in quantities proportional to the amount of burned fuel. The CO_2 is released into the atmosphere, where it contributes to an increase in the greenhouse effect. If the fuel is fossil HC-based (crude oil), the total amount of CO_2 is added to the atmosphere and an ever-increasing amount is the result. The speed of increase depends on a tradeoff between the total amount of burned HC and the vegetal photosynthesis, which decomposes CO_2 and releases O_2. The amount of released CO_2 in modern societies is largely superior to the available vegetal photosynthesis capability. On the other hand, if an alcohol fuel such as ethanol is extracted from a vegetal base, the amount of CO_2 released by burning ethanol as a fuel is compensated by the regrowth of the plants used, which will absorb a similar amount of CO_2. Therefore, the ethanol cycle can be considered as CO_2-neutral, if the necessary energy for distillation is obtained from vegetal raw material, for example, sugar cane pulp. Moreover, even if oil or coal-based power plants supply the industrial energy for the distillation, the overall improvement (decrease) with respect to crude-oil-based fuels is better than 75%. The use of ethanol

* Corresponding author. Tel.: +55 31 8642 3698.
E-mail address: baeta@demec.ufmg.br (J.G.C. Baêta).

http://dx.doi.org/10.1016/j.enconman.2015.08.041
0196-8904/

Nomenclature

EDI	ethanol direct injection
EXX	blend containing XX % of ethanol
PFI	Port Fuel Injection
CO_2	carbon dioxide
HC	hydro carbon component
NO_X	nitrogen oxide
CR	compression ratio
EGR	Exhaust Gas Recirculation
EPA	Environmental Protection Agency (USA)
CFD	computational fluid dynamics
NCM	numerical computational modeling
N–S	Navier–Stokes
ALE	arbitrary lagrangean Eulerian
SG	spray guided
Tr_z	Swril coefficient in Z axis
Ca	average axial velocity
y	coordinate
v	velocity
i	number
CA	crank angle
VVT	variable valve timing
ECU	electronic control unit
FTP	Fiat Powertrain Technologies
NVH	noise vibration harshness
SMD	Sauter mean diameter
PN	particulate number
COP	united nations climate change conference
DI	direct injected
NA	Naturally Aspirated
RON	research octane number
VEM	virtual engine model
GDI	gasoline direct injection
HCCI	homogenous charge compression ignition
Tr_y	tumble coefficient in Y axis
$D_{cylinder}$	cylinder diameter
x	coordinate
u	axial velocity
w	transverse velocity
n	number
TDC	top dead center
λ	lambda
IMEP	indicate mean effective pressure
BMEP	Brake Mean Effective Pressure
L/D ratio	lift per diameter ratio of directed injector
D_{10}	arithmetic mean diameter
ORNL	Oak Ridge National Laboratory (USA)
UFP	ultrafine particles

reduces the CO, HC and NO_X contents in exhaust gases as compared to the equivalent gasoline combustion. Ethanol fuel represents therefore an important means of achieving the commitments fixed first in the Kyoto protocol and more recently by the latest COP agreement to reduce CO_2 emissions. Furthermore, the large variety of raw material (plants), from which ethanol can be produced makes it possible to supply from local agricultural areas. This means energy supply independence in the event of international political crises.

Pure alcohol fuels have been shown in the past in numerous works to offer some significant benefits over gasoline amongst other fuels, as reported by EPA [1]. Their high octane rating provides the ability to operate even low-pressure Port Fuel Injected (PFI) engines at higher compression ratios avoiding important pre or post-ignition problems [2]. Furthermore, its greater latent heat of vaporization offers a higher charge density [3] and its higher laminar flame speed enables it to be run at leaner and more diluted air–fuel mixtures [4,5]. As alcohol fuels generally decrease pollutant emissions under hot engine conditions compared to gasoline and by using renewable feed-stocks, a significant decrease of greenhouse gas (CO_2) has contributed to the important success of flex-fuel vehicles in both North and South America, as well as in Europe [6,7]. Typically these flex vehicles of first and second generations are powered by small (1- to 1.4-l) to middle (1.9- to 2.2-l) sized displacement engines optimized for ethanol use (using materials resistant to alcohol). The Direct Injection (DI) approach is an ideal system for an ethanol engine as the fuel properties enable high Compression Ratios (CR) in the range of 12–14:1. If the combustion chamber design is adapted to DI-approach this can significantly decrease knock occurrence and generate a more precise fuel metering compared to a PFI layout. If the DI approach is applied to a turbocharged, down-sized, down-speeded engine a significant decrease in engine friction and pumping losses is possible, as well as a reduction in exhaust emissions and a recovery of the power output. This leads to a significant improvement in brake thermal efficiency. During the study of a 4-cylinder 1.4-l engine fitted with a single stage turbocharger and running on hydrated 100% Ethanol (E100) fuel, which is a regular fuel in the Brazilian market, it was discovered that the down-speeded properties of the engine enabled a change from a 4-valve intake layout to a 2-valve high-swirl flow structure maintaining a high power output. This leaves room for a significant cost reduction and puts the EDI down-sized and down-speeded engine in a range where it can rival the diesel engine power performance at a lower cost. A further aspect of this engine is its capability of replacing a medium to high displacement engine [8], and with adequately redesigned gear ratios installed into a car, which was originally fitted with a much bigger Naturally Aspirated (NA) engine. The replacement of a NA 2.4-l engine by a boosted 1.4-l engine is initially studied. Several researchers have documented the benefits of down-sizing [9–12]. Afterwards, based on the low-end torque obtained, it was decided to extend the power output by a replacement of the single turbo with a twin-stage turbocharger. By this means, it was possible to suppress any turbo-lag and to replace an even bigger NA 3.0-l V6 engine. Besides the twin-stage, other strategies aiming at suppressing the turbo-lag occurrence were carefully investigated [13]. By this last replacement, a 53% down-sizing was achieved. The properties of hydrated E100 fuel compared to E85 make it possible to extend the spark authority to very high Brake Mean Effective Pressure (BMEP), producing additional brake thermal efficiency gains. Furthermore, the increased CR allowed by the use of hydrated ethanol fuel expands the range of diluted operation. The use of increased levels of Exhaust Gas Recirculation (EGR), which in the present case is a cooled EGR approach, decreases the level of NO_X emissions [1] and suppresses the occurrence of pre-ignition phenomena [14,15].

1.1. Basic fuel properties

Ethanol has a high octane rating and is often used as an octane improver in reformulated gasoline blends. The RON values for ethanol are from 105 to 109, as compared to 91 to 99 for gasoline [16,17]. Other qualities of ethanol, such as its low heat value and Reid vapor pressure, as well as its latent heat of vaporization, which is 2.4 times higher than that of gasoline and its increased laminar flame speed makes it an ideal match for use with both

Table 1
Basic fuel properties. Source Petrobras (2011).

	Gasoline	Hydrous ethanol			
	E25 (H0)	(H30)	(H50)	(H80)	(H100)
Density (kg/m^3)	748.2	754.9	779.2	797.7	808.7
MON	85.1	88	89.7	91.6	91.8
RON	97.3	>100	>100	>100	>100
Carbon (%)	73.3	64.3	59.5	53.9	50.7
Hydrogen (%)	13.7	13.4	13.3	13.1	13
Oxygen (%)	13	22.3	27.2	33	36.3
Fuel formulation	$CH_{22}O_{0.13}$	$CH_{25}O_{0.26}$	$CH_{27}O_{0.34}$	$CH_{29}O_{0.48}$	$CH_{30}O_{0.53}$
Heat value (MJ/kg)	38.92	34.68	31.84	27.59	24.76
RVP (kPa)	55.9	52.5	47.2	33	15.4

PFI and DI approaches to increase efficiency gains and decrease NO_X raw emissions. Furthermore, attention should be drawn to the charge cooling effect of ethanol. This is a predominant factor when the search is directed towards an increase in CR and turbo boosting. As the knowledge of variations in chemical composition and flame speed behavior is crucial to understand why experimental results might vary between the Brazil, the USA or Europe the data are given in Table 1 and Fig. 1. Table 1 indicates basic fuel properties and Fig. 1 the laminar flame speeds for gasoline and E100 versus the exhaust gas equivalence ratio.

2. Experimental setup

The research described below has the purpose of demonstrating the feasibility of cleaner more efficient engine technologies. This study defines an engine architecture that fully exploits the ethanol potential in order to match E22 fuel mileage for Brazilian market applications and having the same performance index. The first phase comprises the development of a PFI engine layout that is tested both on an engine test rig and installed in a prototype car to evaluate the technology boundaries. The second phase covers the implementation of an ethanol DI layout in order to extend and evaluate further efficiency gain and its cost-effectiveness. The study answers the question whether it is possible to make an ethanol engine using hydrated E100 producing the same volumetric consumption and torque curve as its gasoline (gasohol E22) counterpart. Several engines were used for this work. As a baseline for the down-sized engine a 1.4-l 16-valve passenger car engine was used in both a single cylinder transparent version and a multi-cylinder version for engine test rig experiments and for installation in a prototype car originally fitted with a 2.4-l NA-engine. Initially, the 1.4-l multi-cylinder engine was studied in NA-conditions, then fitted with a single stage adapted turbocharger, and finally with a twin-stage electronically controlled turbocharger. To make clear to readers with less knowledge of current automotive experimental test capabilities Figs. 2 and 3 indicates some of the more sophisticated tools. Fig. 2 shows the single cylinder and the multi-cylinder layouts of the 1.4-l engine. Fig. 3 shows the twin-stage compressor design.

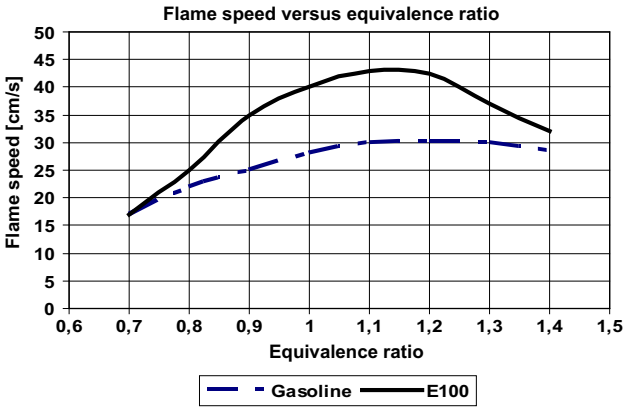

Fig. 1. Laminar flame speed for gasoline and E100. [Source EPA].

The specifications of the baseline 1.4-l engine are listed in Table 2. To adapt the baseline engine particularly to ethanol use a series of hardware modifications were performed.

Fig. 4 shows the logical flow chart of the use of all the different research supports. To rapidly obtain the designs of the modifications a high-level 3-D numerical simulation tool was used before the physical modifications were applied. A short description of the applied tool will enable a better understanding of the performance of the tool used.

3. Simulation tool structure

The numerical simulation tool used was a dynamic 3-D CFD, thermodynamic and chemical tool applied to the entire engine structure contained within the boundaries of the inlet throttle body and the exhaust pipe junction on the upstream side of the catalytic converter. Fig. 5 shows an example of the delimitation of the 3D computation area, also called a VEM.

As the main topic of this paper is not that of numerical simulation tools, only a few comments will be made about the usage and the reliability of the used VEM approach. Whenever a totally predictive research work is made, such as the analysis of new combustion chamber geometry or the impact on the dynamic mixture preparation of a new fuel injector atomizer, it is very important that the user/researcher knows the validity and limits of all the assumptions related to the models and sub-models involved in the computations. As this entire knowledge is only available in very few commercial computation codes, the VEM software basis used for the present development is a non-commercial company code. This code, the NCM-3D, has been continuously co-developed and refined for more than 25 years by the authors in collaboration with the Tor Vergata University in Rome (Italy). During this time the code was successfully tested and used for system development on more than 30 different real engines, representing a very wide range in displacement and power output (from 5.9-l 4-cylinder aircraft, 10-cylinder F1, middle to small displacement SI and CI and down to 50 c.c. two-stroke engines [18–23]. The code was originally developed as a high performance simulation tool for optimization of the design of GDI-based combustion chamber layouts and mixture preparation components such as fuel injectors for a lean stratified combustion approach. The original version, in which the resolution of the governing 3D N–S equations, is based on the well-known KIVA-3V approach. The KIVA approach was originally developed by the Los Alamos Laboratory [24,25]. The approach employs a finite volume approximation in a Cartesian or cylindrical reference system in which a

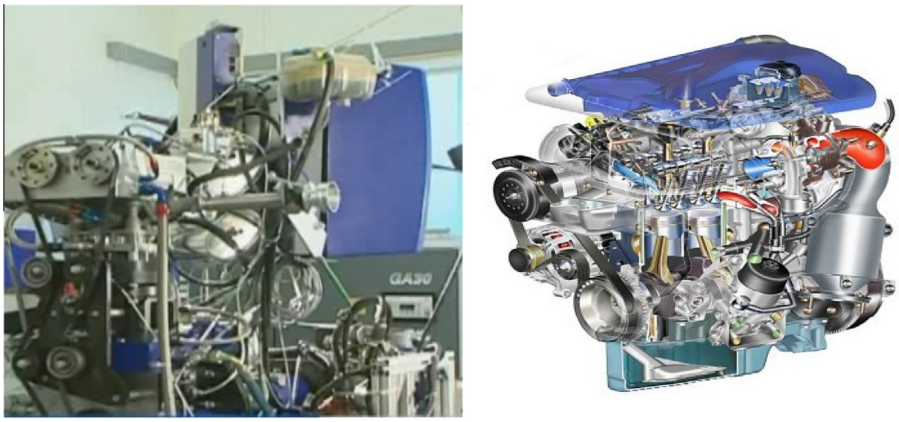

Fig. 2. Single and multi-cylinder engine layouts.

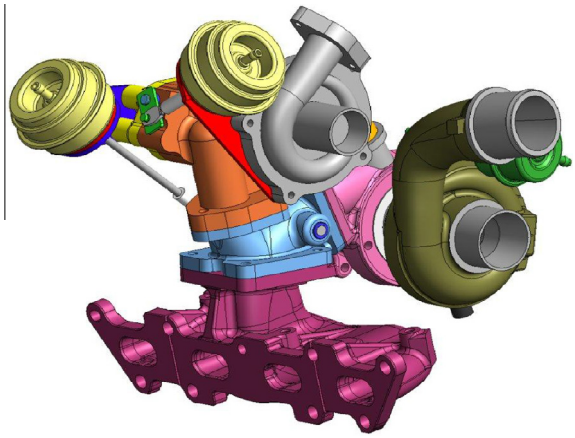

Fig. 3. Twin-stage turbo charger design.

multi-block structured grid is generated. The NCM-3D uses a modified κ–ε turbulence model, accounting for compressibility effects, during the Arbitrary Lagrangian–Eulerian integration of the averaged N–S equations. The code was successively modified by including high-level flexible dynamic grid control (one single grid is used for the entire engine cycle) and in the later rewritten versions by adding compatibility with Pentium high-speed processors and complete multi-node parallel processing capability. The specific physical models implemented in the code enable full 3D computation of both gas and fuel spray dynamics, including atomization, vaporization of multi-components fuel, internal droplet ballistics and fuel/wall interaction, as well as the complete combustion phase including auto-ignition and computation of post-combustion products (HC, CO, CO_2, NO_X, Particulates). In particular, the wall/liquid interaction models take into account the complete phenomenon of wall-film deposit, droplet propagation and bouncing as well as film undercutting phenomena and local surface vaporization. To avoid any type of parameter-tuned model approach a lot of care was taken with each implemented model to make its layout depend on physical relationships only. For precision considerations can be said that inside the virtual computation space no uncertainty is present between runs with unchanged parameters. The above mentioned numerous tests with a large number of different real engines have shown that the correlation between computed results and the physical engine results for this simulation tool has an overall precision of ±5%.

The above-mentioned details were highlighted to make understandable to what extend the impact on the mixture preparation and propagation of small changes in components and combustion chamber design can be predicted within a relatively short time frame (about 8 h of CPU time on an 8 node cluster for one complete engine cycle). This enables bias of the produced combustion event in a desired direction.

Table 2
Baseline engine specifications.

Engine type	4 Cylinders–4 stroke
Stroke	84 mm
Bore	72 mm
Displacement	1368 cc
Compression ratio	9.3:1
Number of valves per cylinder	4
Fuel type	Gasoline or ethanol
Injection system	PFI
Turbocharger over-boost	0.35 bar

4. General combustion approach

Before presenting details of all the different measurements implemented on the baseline engine for the reduction of fuel consumption and engine-out emissions, a general discussion of the philosophy of the combustion approach has to be presented. The overall idea of the combustion pattern produced by the baseline engine is to benefit from the possible system as well as layout optimizations. As the baseline engine is a 1.4-l PFI engine the primary optimization process is related to this layout. Traditionally, this engine type suffers from part-load pumping losses caused by throttle control, relatively low CR-values to avoid engine knock, mostly stoichiometric mixture preparation required by 3-way catalysts and finally a production of high levels of CO_2, unburned HC and high NO_X in the exhaust gas [26].

Several researchers have suggested solutions to these problems, such as introduction of DI mixture preparation in both stoichiometric and lean stratified combustion modes [24] and use in the low-load area of a HCCI approach [27,28]. For this presentation of an ethanol engine the EDI system considered is a SG layout, which offers the best fuel economy approach [29]. The lean stratified mode as well as the introduction of HCCI, which require specific and not always very reliable after-treatment technologies, were not considered, as the focus of this research was not on catalytic converter concepts. In this discussion the focus is on a wide set of layout optimizations. To analyze initially the hardware design of the combustion chamber as well as its upstream and downstream side the above-mentioned simulation tool NCM-3D was used intensively. An example is the research for an optimal

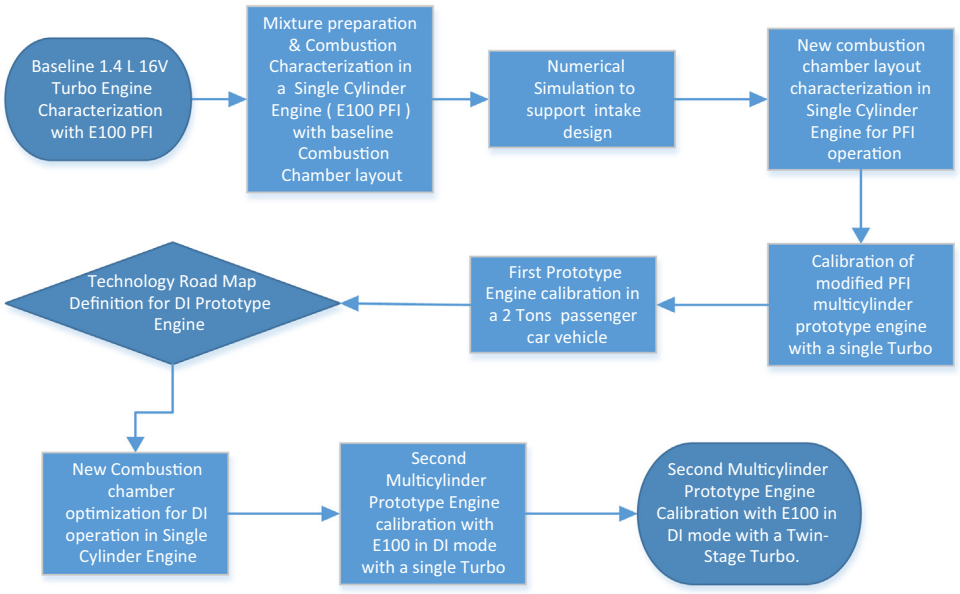

Fig. 4. Research program flow diagram.

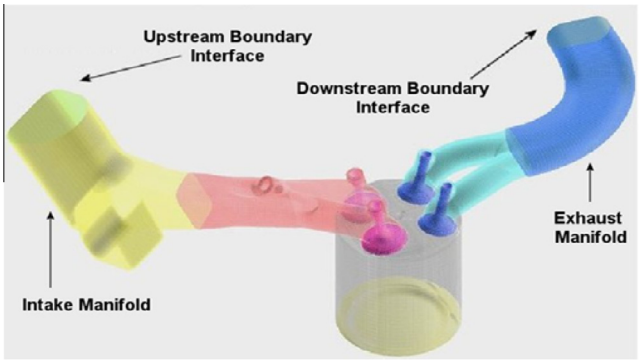

Fig. 5. 3-D VEM computation mesh.

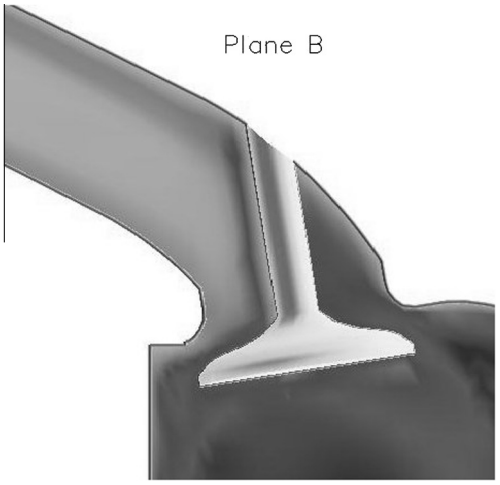

Fig. 6. High tumble port.

swirl/tumble compromise. The in-cylinder tumble and swirl motion ratios are defined as follows for a cylinder axis denominated "Z":

Tumble around the *Y* axis:

$$Tr_y = \frac{\pi}{4} \cdot \frac{D_{cylinder}}{c_a} \cdot \frac{\sum_{i=1}^{n}(-w_i x_i)}{\sum_{i=1}^{n} x_i^2} \quad (1)$$

Swirl around the *Z*-axis:

$$Tr_z = \frac{\pi}{4} \cdot \frac{D_{cylinder}}{c_a} \cdot \frac{\sum_{i=1}^{n}(v_i x_i - u_i y_i)}{\sum_{i=1}^{n}(x_i^2 + y_i^2)} \quad (2)$$

Mechanically, the tumble motion is favored by "high" intake ports with an axis pushed towards the cylinder axis. Fig. 6 shows an example of such a port design. High-tumble motion is used in high-speed, high-performance engines (i.e., racing engines). The swirl motion is favored by "flat" intake ports with an axis as perpendicular as possible to the cylinder axis [30]. High swirl motion is used for low speed engines where the higher head loss of a flat port is less important due to the comparatively lower air velocity in the port. Fig. 7 shows an example of such a port design. In particular, for our present research the swirl component is of interest as the swirl component in the combustion chamber decays much slower than the tumble component. The choice of the optimal

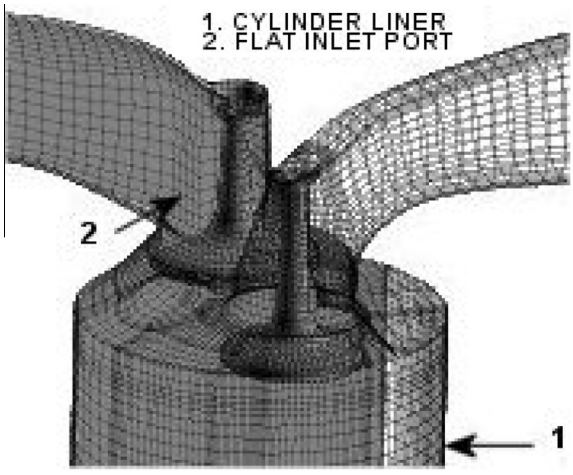

Fig. 7. Flat swirl port.

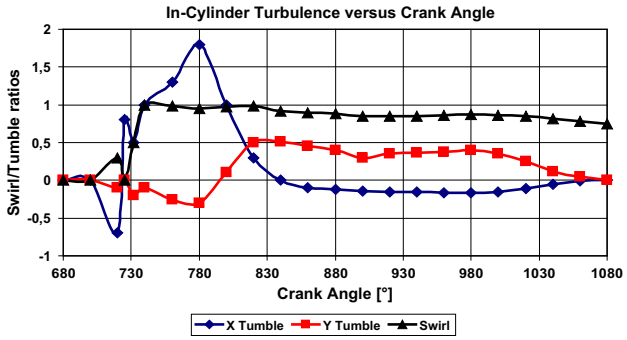

Fig. 8. Swirl and tumble ratios versus CA.

intake port design was defined by the numerical simulation tool by researching for the maximum swirl ratio and the slowest decrease of this ratio.

This is important for the adjustment of the burn duration (window) of a down-speeded engine. Details of this are addressed in the engine results section. Fig. 8 shows an example of the computed (NCM-3D) decays of the tumble and swirl ratios versus the CA-position after TDC (720°) for a given port design. Further design enhancements for increased swirl motion such as valve seat shrouding as well as DI and off-centered position of the spark plug, will also be addressed in the next sections.

Finally, the introduction of a cooled EGR-system to stabilize the combustion temperature (engine efficiency) and a VVT-system to enable eventual negative overlap are supplementary measures for the reduction of fuel consumption and engine-out emissions [31,32]. In this way, the de-throttling strategy were also adopted to make possible a significant pumping loss reduction at partial load operation. To take full advantage of the above-mentioned measures our general combustion approach therefore requires a turbocharged, down-sized and down-speeded baseline engine layout.

5. Implementation of physical hardware changes

The computations by the numerical simulation tool (NCM-3D) demonstrated that a residual free volume above the piston roof of only 31 cm^3 at TDC is necessary to provide a new CR of 12.03:1 better suited to ethanol fuels. The VEM permitted the design of a new piston roof adapted to obtain the desired CR. Fig. 9 shows the difference in the roof designs. Furthermore, it was clear from the computations that to maximize the thermodynamic efficiency for the use of a turbocharger the exhaust manifold had to be redesigned with a smaller volume compared to the original version (decrease of approximately 35% – see Fig. 10).

For the engine two cylinder heads were prepared, a 16-valve version (original for the PFI version) and an 8-valve version. Some modifications were introduced to the cylinder head designs. The profile of the intake ports was modified on both heads to a flat form that generates a high tangential gas motion (inclined swirl). On the 8-valve head, the intake valve diameters were increased by 50% and the exhaust valve diameters by 40% of the bore diameter. To enhance the gas swirl motion behavior further on both

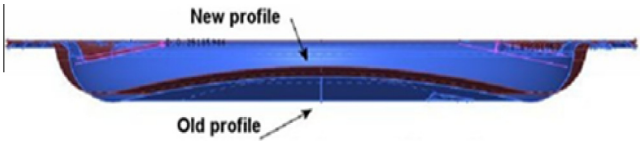

Fig. 9. Piston roof profiles.

Fig. 10. Reduced volume exhaust manifold.

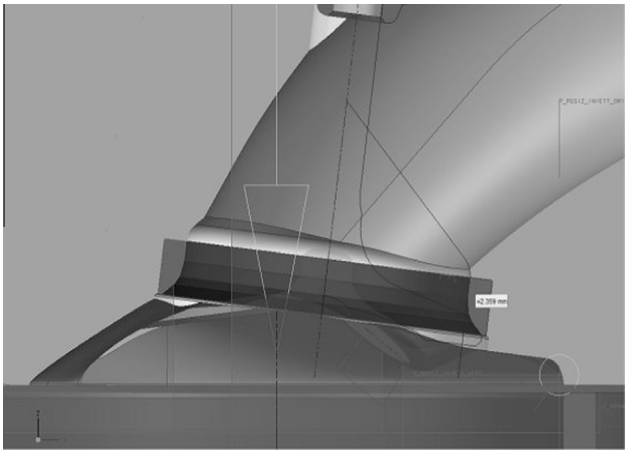

Fig. 11. Reduced valve seat thickness.

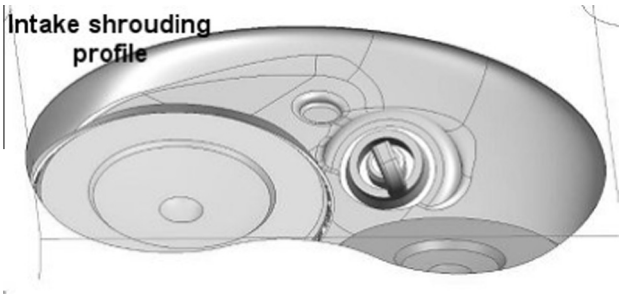

Fig. 12. Example of valve shrouding profile.

heads, the design of the intake valve seat was made to decrease the seat thickness as much as permissible, according to robustness criteria (Fig. 11). The layout of the roof profile of the heads was non-symmetrical as the area around the intake valve seat had a 1.5 mm shrouding profile and that around the exhaust valve a 3.5 mm profile (Fig. 12).

Finally, to take better advantage of the new strong swirl flow field, the spark plug position on the 8-valve head was repositioned at 10.7 mm away from its original center position (Fig. 13).

This also procured space for the mounting of a direct fuel injector in a central position, which is well suited for the application of a SG mixture preparation approach for the EDI system introduced later.

5.1. Some comments on the 8-valve head performance

By the application of the above-mentioned measures to the 8-valve baseline head a peak swirl ratio of approximately 3.0

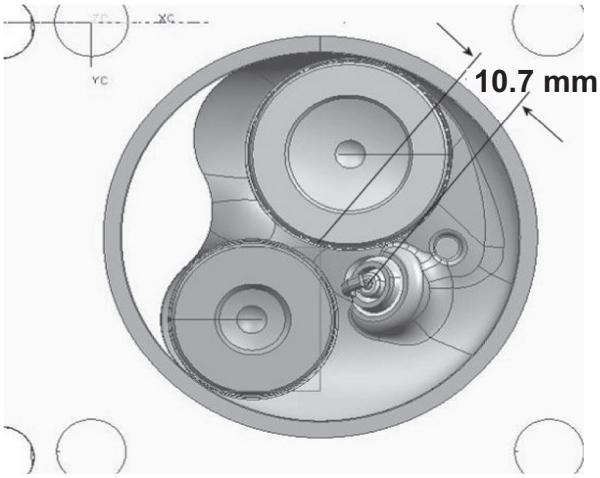

Fig. 13. New spark plug position.

was achieved. The advantage of an 8-valve head is related to the fact that the use of a down-speeded layout enables high gas cycle engine efficiency. In fact, the pressure drop across the valves increases proportionally to the engine speed for the same volumetric efficiency when the engine speed is increased. For the down-speeded engine, the nominal lower speed range will compensate the increase in pressure losses induced by a high swirl motion, and therefore the use of preferential swirl instead of tumble becomes interesting. A high swirl level has the advantage of reducing the cycle-to-cycle variation of the combustion pressure. Apparently, for the down-sized and down-speeded layout, there is no significant advantage in using a 4-valve layout compared to the above-mentioned 2-valve layout, but the latter has a significant cost reduction potential for the cylinder head at equivalent performance levels. It must be recalled that the single camshaft basic layout necessary for the control of the 2-valve version was easily, and with only little extra cost, replaced by two concentric shafts; one for the intake lobes and the other for the exhaust lobes. Through this approach a fully flexible variable control of the valve timing is possible (VVT). The shaft phase between the intake and exhaust cams is electronically controlled, and enables full advantage to be taken of the cooled EGR system. Actually, the possibility of addressing negative valve overlap conditions makes it possible to obtain internal EGR to very precisely control the combustion peak temperature (NO_x), as well as charge heat diffusion/loss to the liners [33].

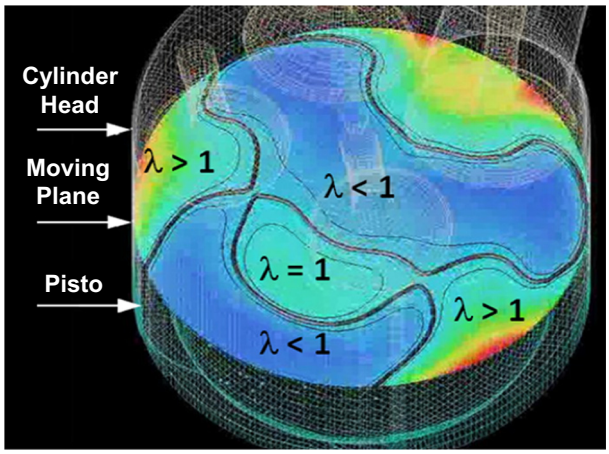

Fig. 14. Color map in moving in-cylinder plane. (For interpretation of the references to colour in this figure legend, the reader is referred to the web version of this article.)

6. Results from the different engine layouts

The performance of the flow enhancement features on the cylinder heads was controlled and well confirmed by the numerical simulation tool results. To illustrate the type of results given by the simulation tool, a CA resolved overall analysis of λ-values present in a moving plane, which is positioned halfway between the cylinder head gasket plane and the piston roof. This moving plane indicates the temporal position of mixture in the combustion chamber. Fig. 14 shows the map produced by the analysis at a CA-value of 80° before TDC of compression for the PFI version of the baseline 1.4-l engine.

To enhance the mixture distribution quantitatively inside the cylinder a further analysis was performed by a computation module, which monitors the instantaneous λ-values in 6 points distributed on a circle with center on the cylinder axis and having a radius of 80% of the bore. Through the points three planes separated by 60° can be identified, all passing through the center point of the spark plug gap. Fig. 15 shows the corresponding scheme. This kind of representation is of particular interest at the CA-value corresponding to the instant of spark release (in the present example at 26° before TDC).

This observation enables a precise evaluation of a homogeneity index prior to ignition. In correlation with Figs. 14 and 16 show the lambda distribution in the three planes indicated by Fig. 15.

The derived homogeneity index is defined as:

$$1 - \frac{\lambda_{MAX} - \lambda_{MIN}}{\lambda_{MAX}} \tag{3}$$

The defined homogeneity index offers the important advantage of being totally independent of the subjective interpretation of a physical observer. The average value for the analyzed low-load points of the homogeneity index is 0.76 (ideal is 1), which is quite a good performance.

6.1. Engine test rig results

The two engines, the down-sized 1.4-l turbocharged and the 2.4-l NA, were at equal torque and power conditions compared at the engine test rig. The engines were tested in a speed range between 1500 rpm and 4000 rpm for the down-sized engine and up to 6000 rpm for the 2.4 l engine. The load range is from low load (~500 kPa BMEP) to full load. Both the single cylinder and multi cylinder test rigs are AVL latest generation test rigs combined with AVL-Puma analyzers and Concerto/Indiset data acquisition equipment. The overall uncertainty of this equipment is when properly calibrated prior to the measurement phase within the limits of ±0.7%. In particular, the results from the down-sized 1.4-l engine

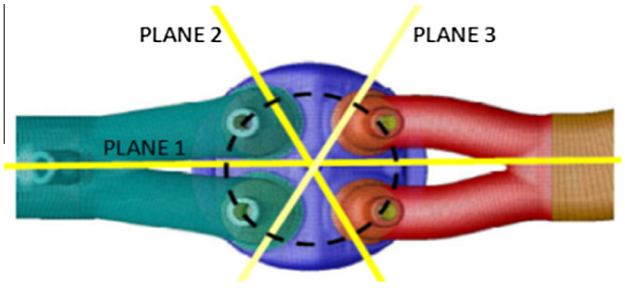

Fig. 15. Planes in which the instantaneous λ-value is monitored.

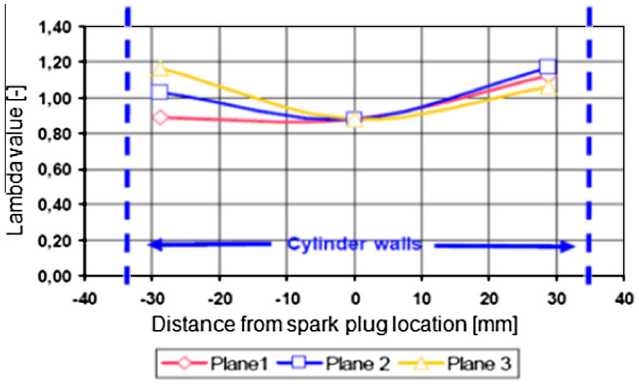

Fig. 16. In-cylinder λ-distribution.

fitted with the two-stage turbocharger are of interest. Fig. 17 shows the engine with the two turbochargers.

Fig. 18 indicates the compressor pressure ratio delivered from the low-pressure and the high-pressure stages as well as the combined action of the two stages over the engine speed range. The entire system is efficient as the pressure ratio is between 2.6 and 2.8 over a speed range between 1000 rpm and 5000 rpm. The torque produced with the twin stage system is very good.

Fig. 19 shows the twin-stage compressor pressure map. The full line with square marks indicates the engine work line.

As shown in Fig. 20, an excellent flat torque performance of approximately 290 N m was obtained between 1750 rpm and 3500 rpm with a peak value of 300 N m.

This performance was obtained with the use of hydrated Brazilian 100% Ethanol (E100) fuel.

Figs. 21a and 21b show a graphic example with related numerical data recorded in the cylinders during combustion of the down-sized engine at 3500 rpm. The data indicated at the figure correspond to the single stage compressor version (high-pressure stage alone) and show that even in this version the down-sized engine performs very well. Several comments are important. The maximum compression pressure and IMEP values are excellent, respectively 160 bar and 29 bar. Furthermore the burned mass fraction between 10% and 90% is accomplished in a CA-window, which oscillates between 22° and 24°. This behavior is not far from the ideal behavior of a CA-window of 30° found in the works published by MIT [34]. In this work is stated by J.B. Heywood, amongst others, that if the peak efficiency for the 10–90% burn ratio lies within the 30° CA-window then a regular well-controlled monotonically running combustion process will be the result. This is important because if the imposed in-cylinder swirl flow field is tuned to dissipate in synchronization with the burn duration a maximum efficiency is achieved and thereby an increase in engine performance and a decrease in fuel consumption. Fig. 22 shows the data obtained by the MIT team.

Fig. 17. Engine fitted with two-stage turbo.

7. Introduction of high-pressure DI injection

For the DI approach a primary numerical simulation analysis was adapted to a high pressure multi-hole injector for which the spray pattern was made compatible with a SG layout. A very important feature of DI is the charge cooling effect of the fuel directly injected in the combustion chamber where the total vaporization takes place. This, in conjunction with the cooled EGR approach, helps to stabilize the temperature field in the combustion chamber. The SG layout is the approach, which take full advantage of the flow precision of DI injection and procures the possibility of multiple injections during an engine cycle [35]. The SG DI-approach decreases the CO and unburned HC emissions but the influence on the NO_X emissions is weak. Furthermore, the low variability of the position of the different lobes of the spray is fundamental for a SG layout, as the spray border must be positioned between 0.5 and 1.5 mm from the spark plug gap zone in which the spark release is performed. Fig. 23 shows the defined multi-hole injector. The test series performed by the numerical simulation tool suggested that the best fit was obtained by a 5-hole fuel atomizer structure composed of a narrow layer of two sprays and a wider lower layer of three sprays. The static flow of the injector is approximately 11 g/s at 10 MPa and the L/D-ratio for each hole of the thin-plate atomizer was kept as low as 1.1. Fig. 24 shows the design obtained by use of the numerical simulation tool for the installation of the 5-hole injector in a center position with respect to the spark plug where the two lobes of the upper layer pass on each side of the spark plug electrode.

Fig. 25 shows a frontal and a bottom view of the overall spray pattern formed by the five lobes. The pictures correspond to a time frame of 0.9 ms after start of injection. At 10 MPa nominal test pressure the injector atomizer produces an average droplet size distribution at 50 mm from the injector tip characterized by a D10 of 15 μm and a SMD of 65 μm. Already the simulation tool indicates the increase in performance obtained by a change from Port Fuel Injection to direct injection. The compression ratio of the direct injected engine was raised to 14:1.

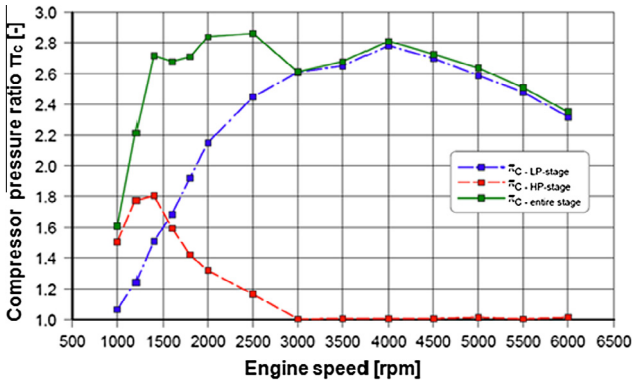

Fig. 18. Two-stage compressor performance.

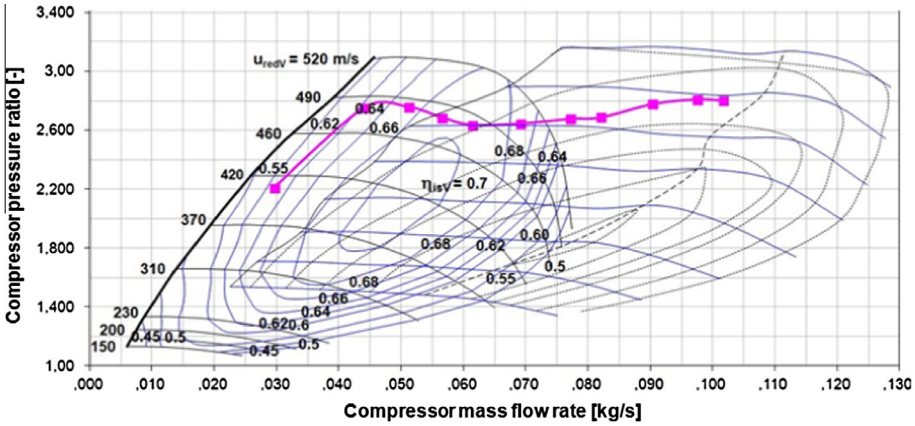

Fig. 19. Twin-stage compressor pressure map.

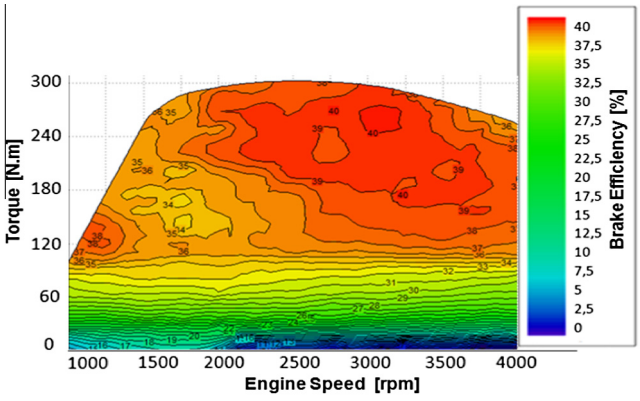

Fig. 20. Torque and brake efficiency versus engine speed.

Fig. 26 shows the corresponding combustion pressure trace at a load point of 2000 rpm and 4 bar IMEP in which the comparison of the DI-based combustion to the PFI-based combustion reaches an 18% higher peak value of 62.5 bar at 2.5° CA after TDC.

On the engine test rig the introduction of the DI layout produced 3% increase in peak combustion pressure of the down-sized turbocharged engine at 5500 rpm and a BMEP of 32 bar. Experimentally, it was detected that to push the BMEP further than 32 bar, the cooled EGR system is mandatory to avoid any pre-ignition mainly, at low speeds where the flame propagation is quite low.

8. Comparison with high displacement naturally aspirated-engine

To get comparative information at equal torque and power conditions between data of the down-sized baseline engine and the 2.4-l NA-engine, both engines were mounted on the engine test rig. Fig. 27a shows the performance of the baseline down-sized and down-speeded engine equipped with a single stage turbocharger for comparison with the 2.4-l NA engine.

Fig. 27b shows the comparative performance of the 2.4-l NA-engine under similar conditions. The data are obtained by fuelling the 1.4-l engine with E100 and the 2.4-l NA-engine with E22. The maximum power output is similar for both engines (141 kW) with a corresponding torque around 180 N m and 200 N m, but the 1.4-l engine produces these values at 3800 RPM, whereas for the 2.4-l engine the values are reached at 6000 RPM.

Fig. 27c shows the power performances of both engines in the same graphic. It can be seen that the maximum power delivered by the down-sized and down-speeded 1.4-l engine equipped with the single-stage compressor (Fig. 20) is higher than its higher displacement counter parts at the same speed. The 2.4 l NA-engine is originally mounted in the vehicle chosen for mounting of the down-sized 1.4-l turbocharged engine. However, this same vehicle is equally available with a 3.0-l NA V6 engine. As all three engines mount in the same vehicle frame it is meaningful to compare the down-sized engine to both high displacement engines. Comparison with the 2.4-l engine shows a down-sizing capability of 42% by the substitution with the 1.4-l engine. This same data for the 3.0-l

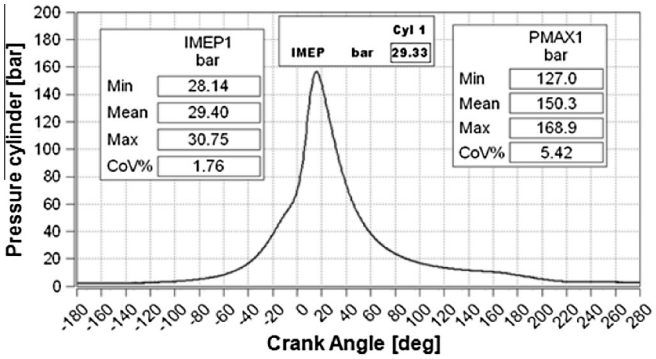

MBF 50% Cyl. [deg]
12.88
MBF 50-10 Cyl.1 [deg]
8.81
MBF 90-50 Cyl.1 [deg]
13.61
MBF 90-10 Cyl.1 [deg]
22.43

Fig. 21a. Cylinder pressure data.

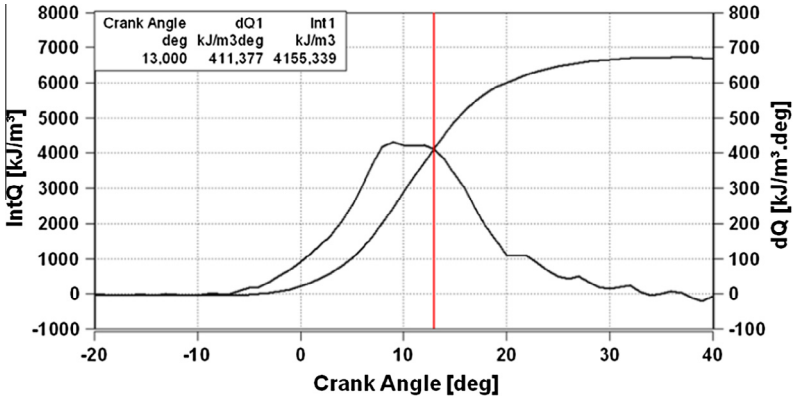

Fig. 21b. Heat Release data.

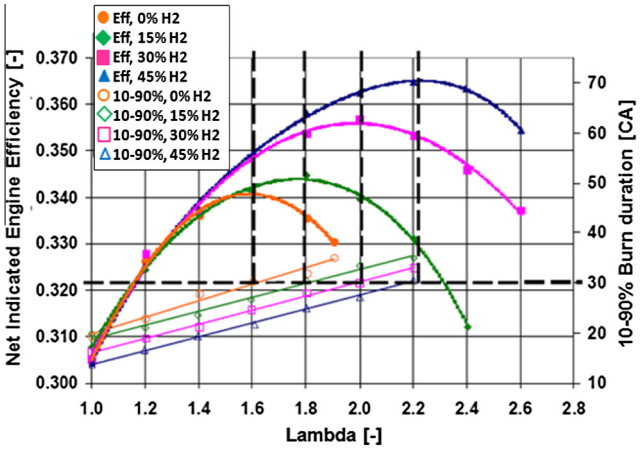

Fig. 22. Engine efficiency and burn duration versus lambda at 1500 rpm – source SAE 2006-01-0229.

Fig. 23. Multi-hole HP injector.

engine is 53% compared to the 1.4-l engine if equipped with a DI-system, a twin-stage compressor and running at 5500 rpm.

In conclusion the 1.4-l down-sized, turbocharged engine offers a high brake efficiency, a more flexible torque availability and plenty of room for gear ratios enlargement when mounted in the vehicle. It should be remembered that the down-sized 1.4-l engine is equally down-speeded, so engine speeds over 4000 rpm are avoided in order to reduce friction and pumping losses as well as to eliminate turbo lag. All the gear ratios were increased for the use of the 1.4-l down-sized turbocharged engine on average by 5–6% and all vehicle tests were performed without changing the tire dimensions. Table 3 shows the main vehicle parameters.

9. Overall experimental results

The mounting of both the 1.4-l down-sized engine and the 2.4-l NA engine in the same vehicle frame was made. For the down-sized and down-speeded engine the gear ratios were adapted to obtain a good drivability and the maximum possible gain in fuel consumption. Also, the software in the ECU had to be adapted to both advanced turbo control and the use of DI injector control, allowing more than one injection per stroke (convenient for stratified operation). The availability of both engines in the same

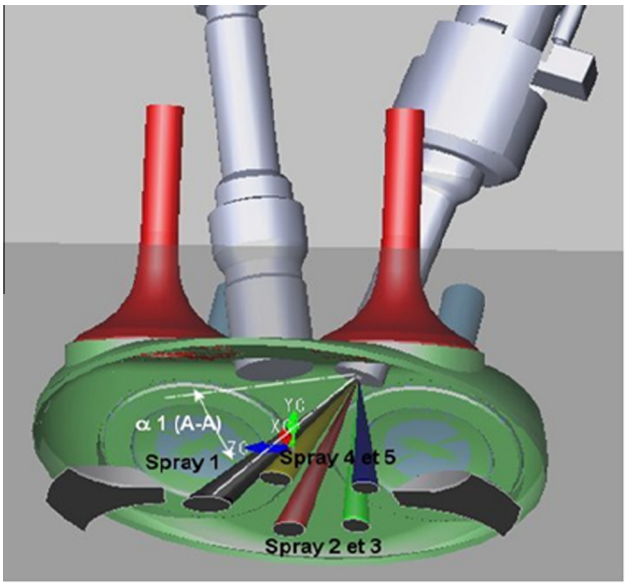

Fig. 24. Installed 5-holes injector for spray guided layout.

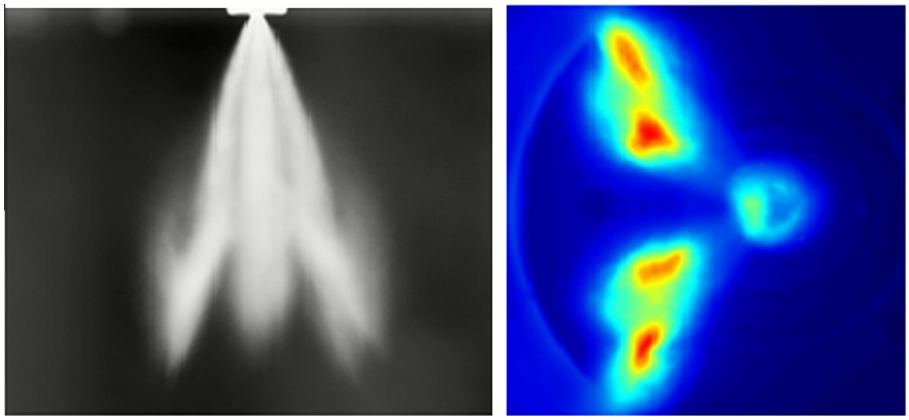

Fig. 25. Frontal and bottom view of the spray.

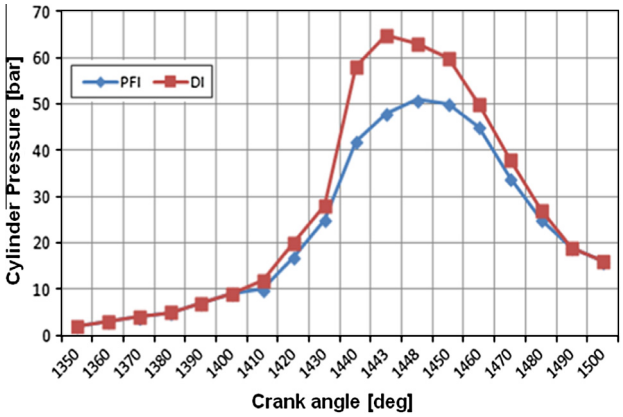

Fig. 26. Comparison of combustion pressure from PFI and DI injection.

vehicle frame permits also the evaluation of the FTP cycle performance. Fig. 28 shows the rather heavy vehicle frame. The comparative vehicle tests were made at the FTP 75-cycle with use of Brazilian hydrated E100 fuel.

In particular, the results obtained in fuel consumption are of interest. The results can be summarized as follows:

- Down-sizing gives a 14% decrease.
- Single camshaft with concentric axes for intake and exhaust lobes (VVT) gives a 2% decrease.
- Optimized combustion chamber design gives a 3% decrease.
- Homogeneous DI gives a 3% decrease.
- A non-stoichiometric mildly leaner stratified DI mixture preparation ($\lambda \sim 2$) gives a 3% decrease.

This adds up to a total gain of 25%. The temperature controlled cooled EGR system gives a further 3% decrease. The comparative vehicle tests made at the FTP 75-cycle by E100 fuel gave an average overall difference on the entire cycles in fuel consumption of 18%. Furthermore due to the improved in-cylinder mixture distribution and reduced internal friction a decrease in HC (18%) and NO_x (12%) emissions was obtained.

The more than 28% of gain in fuel consumption offered by the down-sized turbocharged and down-speeded EDI-engine compensates the traditional fuel consumption penalty of ethanol-fuelled engines (flex engines) and puts this layout in a category, which can rival diesel layouts, but at a lower cost. Not only the fuel consumption data are comparative to diesel performance, but as seen above, the power output is largely competitive with DI diesel layouts. A current turbocharged diesel engine produces a maximum IMEP of approximately 25 bar, whereas this down-sized turbocharged engine reaches an IMEP of 32 bar (see Fig. 27a). This result, which is experimentally obtained and verified, gives an ample window for usage of down-sized engine layouts.

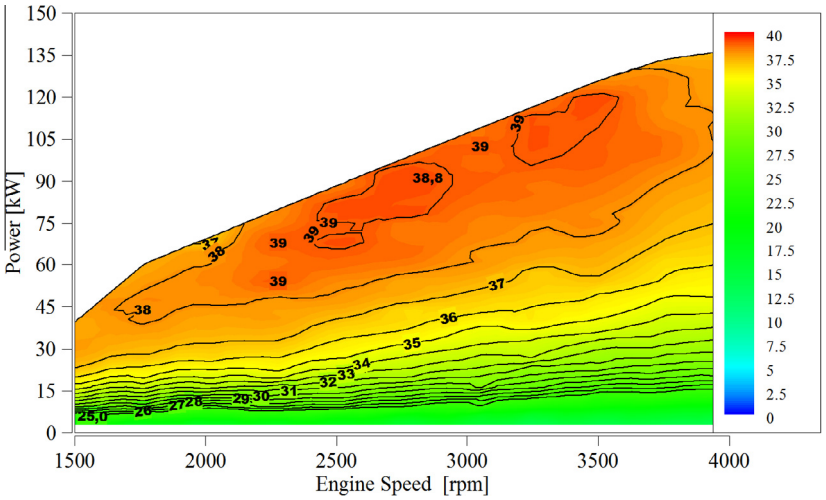

Fig. 27a. 1.4 l engine with single stage turbocharger.

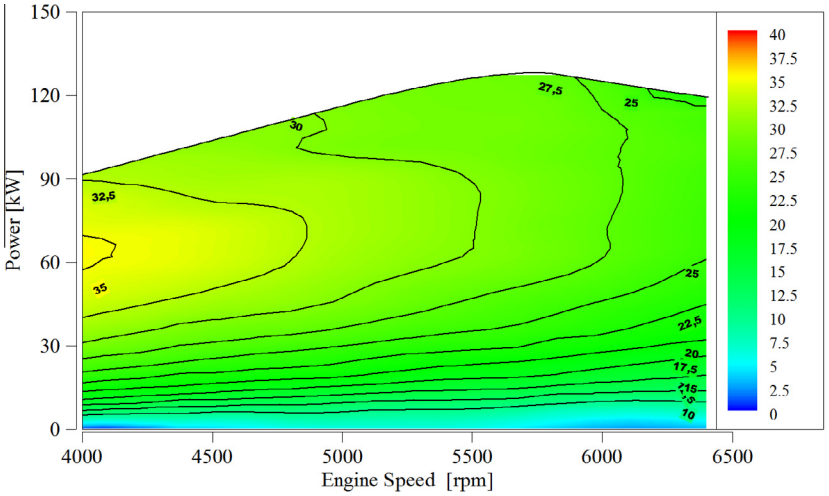

Fig. 27b. 2.4 l NA engine.

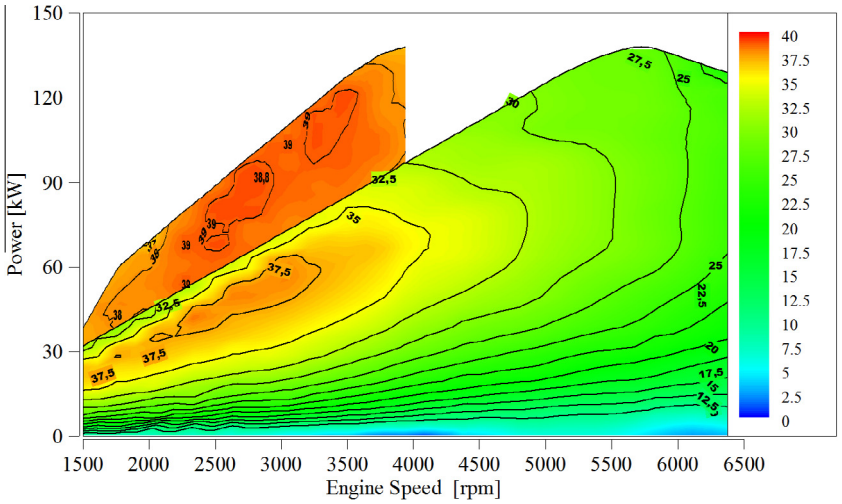

Fig. 27c. Direct comparison between 1.4 and 2.4 l engines.

Table 3
Main vehicle parameters.

Mass M (kg)	1809
Frontal area A (m^2)	2694
Drag coefficient Cd	0.368
Rolling tyre radius R (m)	0.36215
Baseline transmission	4-speed automatic
Baseline transmission ratios	2.842/1.570/1.000/0.690
Optimize transmission	6-speed manual
Optimize transmission ratios	3.909/2.118/1.361/0.978/0.756/0.622
Final drive ratio	4280

As above-mentioned the very flat torque curve produced by the down-sized engine proves its flexibility to replace a high-displacement engine.

It is important to point out that the E100 DI twin-stage turbo engine, in spite of its increased cost, makes it possible to reach better performance in the following areas:

- Due to high-level fuel metering control the cyclic variability is very low.
- An important decrease of the turbo lag at low-end torque adding an increase of 5% in the engine brake efficiency at high load.
- It was also seen that the inertia to reach very high BMEP values at low-end torque during transient operation proved to be the main factor that limits the maximum reachable BMEP. Finally a very important point to commercialize this approach is to comply with the NVH standards in spite of the obtained high

Fig. 28. Vehicle frame.

Table 4
Overall engine performances.

Engine type	Max brake efficiency (%) at [BMEP (kPa)]	Max power (kW) at [speed (rpm)]	50% BMF (CAD) at max power at [brake efficiency (%)]
Standard E22-PFI 3.0l 24v naturally aspirated	35,2: [1132]	195: (6200)	16.9: [28,2]
Standard E22-PFI 2.4l 16v naturally aspirated	38,5: [1159]	141: [5800]	18,3: [27,7]
Baseline E22-PFI 1.4l 16v single turbo	36,1: [1710]	106: [5750]	19,5: [21,2]
Prototype E100-PFI 1.4l 8v single turbo	38,5: [2690]	118: [3750]	13,9: [37,8]
Prototype E100-DI 1.4l 8v single turbo	43,5: [3230]	141: [3750]	11,6: [41,3]
Prototype E100-DI 1.4l 8v twin-stage turbo	44,0: [3250]	208: [5500]	10,1: [42,5]

engine performance. The overall engine performances for all the involved engines in terms of maximum BMEP, power and 50% Burned Mass Fraction (BMF) are listed in Table 4. Also for these values the supremacy of the new down-sized engine is confirmed.

Finally some comments on particulate matter emissions from GDI engines will be carried out. This is probably an important matter for future research works. Recent investigations in Europe and the USA have shown that the modern GDI engines in today's passenger cars can emit more hazardous fine particulate matter than a PFI engine, or even the latest heavy-duty diesels equipped with a particulate filter. The supposed potential impact to public health from these particulates is driving new developments in fuel delivery, controls, and combustion strategies. Therefore the growth in GDI applications means that GDI particulate emissions, though low compared to those of an unfiltered diesel, is now an emerging issue that has researchers examining various approaches to mitigating the problem including new combustion design and engineering concepts, alternate fuels and emissions controls.

Confirmation of the hazard comes via a recent study conducted by researchers at Oak Ridge National Laboratory's (ORNL) Fuels, Engines and Emissions Research Center who found that sample GDI engines emit five to ten times more particulate matter than their PFI counterparts. "The trade off for fuel economy is higher particulate matter emissions, stated ORNL. The particulate size ranges from 5 to 5000 nm in diameter and they can include very heavy, low volatility hydrocarbons and tars". These carbon-based agglomerates can irritate the eyes, nose, throat and lungs, contributing to respiratory and cardiovascular illnesses and even premature death especially among the vulnerable: children, the elderly and those with respiratory conditions.

The particles that are released by GDI engines are smaller and more varied in size than diesel particles. And since these UFP are just on the heavy end of smoke size-wise, they can penetrate deeper into lungs, thus posing greater health risks. Public health authorities are growing concerned about UFP risks in urban areas and near busy highways and major roads.

In Europe, a 5 mg/km (3.1 mg/mi) PM emission limit for GDI engines took effect in 2009 with the Euro 5 standard. The first restrictions for PN emissions come into effect this year with Euro 6. The latter initially limits PN totals to 6×1012 number/km, and then in late 2017 an order of magnitude to 6×1011 number/km. In the U.S., adopting PN standards is under debate.

10. Summary/conclusions

To enhance the combustion behavior of a 1.4-l down-sized turbocharged baseline engine running with hydrated pure ethanol (E100) a study was made to compare the combustion behavior of this engine to series produced high-displacement NA-engines. The purpose of the study was to prove the possibility to substitute these high-displacement engines by the down-sized turbocharged EDI-engine.

Computations made by a high-level 3D numerical simulation approach made it possible to optimize the combustion chamber layout by introducing a new piston roof, redefined intake and exhaust valve seats and diameters and an optimized exhaust manifold volume. Furthermore was adapted a high-performance twin-stage turbocharger. For an implemented DI approach was adapted a high-pressure 5-hole injector for which the spray pattern was made compatible with a SG layout. To get information of the data of the down-sized engine compared at equal torque and power conditions to a 2.4-l NA-engine both engines were mounted on the engine test rig. The torque produced by the 1.4-l down-sized turbocharged engine is an excellent flat torque curve around approximately 290 N m, whereas the torque produced by the 2.4-l NA-engine is inferior ($\sim$200 N m). A 3.0-l NA V6 engine was also tested and its peak torque value is approximately 280 N m. This means that the torque produced by two NA-engines are both inferior to the 290 N m delivered by the down-sized engine in a twin-stage compressor version.

In conclusion the 1.4-l down-sized, turbocharged engine offers a high brake efficiency, a more flexible torque availability and plenty of room for gear ratios enlargement when mounted in the vehicle.

To make a vehicle comparison both the 1.4-l down-sized engine and the 2.4-l NA engine were mounted in the same vehicle frame. The comparative vehicle tests made at the FTP 75-cycle by E100 fuel gave an overall difference on the entire cycles in fuel consumption of 18%.

Furthermore was obtained a decrease in HC (18%) and NO_x (12%) emissions due to the improved in-cylinder mixture distribution and the cooled EGR system.

The more than 28% of gain in fuel consumption offered by the down-sized turbocharged and down-speeded EDI-engine compensates the traditional fuel consumption penalty of ethanol fuelled engines and puts this layout in a category where it can rival diesel layouts, but at a lower cost.

Acknowledgments

The authors gratefully acknowledge Magneti Marelli, MoTeC and AVL for prompt support, providing equipment needed for this research and specially the Brazilian National Bank for Development for funding part of this R&D program.

References

[1] Bakenhus M, Brusstar M. Economical, high-efficiencies engine technologies for alcohol fuels. EPA report; 2005.
[2] Radwan MS. Performance and knock limits of ethanol-gasoline blends in spark-ignited engines. SAE paper 850213; 1985.
[3] Dodge LG, et al. Development of an ethanol-fueled ultra-low emissions vehicle. SAE paper 981358; 1998.
[4] Metghalchi M, Keck JC. Burning velocities of mixtures of air with methanol, isooctane and indolene at high pressure and temperature. Combust Flame 1989;48:191–210.
[5] Marinov NM. A detailed chemical kinetic model for high temperature ethanol oxidation. Int J Chem Kinetics 1999;31(3):183–220.

[6] Pontoppidan M, Bonfiglioli S, Damasceno F, Montanari G. Mixture preparation optimization by CFD of a flex-vehicle (gasoline/ethanol) intake system layout. SAE-Brazil paper; 2004 – No do Resumo 118.
[7] Pontoppidan M, Bonfiglioli S, Montanari, Ewald P. Description of technology development methods used to implement ethanol mixture preparation systems on both automotive and aviation SI-engines. In: Proceedings of XVI ISAF-convention on alcohol fuels, Rio de Janeiro, Section: Infrastructure, Consumption and Environment; November 2006.
[8] Beazley R. EBDI – application of a high BMEP down-sized spark ignited engine. Michigan congress DEER 2009. <http://www1.eere.energy.gov/vehiclesandfuels/pdfs/deer_2009/session5/deer09_beazley.pdf>.
[9] Boretti Alberto. Towards 40% efficiency with BMEP exceeding 30 bar in directed injected, turbocharged, spark ignition ethanol engines. Energy Convers Manage 2012;57:154–66.
[10] Pollice G, Diana S, Giglio V, Iorio B, Rispoli N. Down-sizing of SI engines by turbocharging. In: Proceeding of ESDA 2006–95215, Torino ASME Conference; July 2006.
[11] Lake T, Stokes J, Murphy R, Osborne R, et al. Turbocharging concepts for down-sized DI gasoline engines. SAE paper 2004-01-0036.
[12] Wirth M, Mayerhofer U, Piock WF, Fraidl GK. Turbocharging the DI gasoline engine. SAE paper 2000-01-0251.
[13] Bayomi Nazih N, Abd El-Maksoud Rafea M. Two operating modes for turbocharger system. Energy Convers Manage 2012;58:59–65.
[14] Su Jianye, Xu Min, Li Tie, Gao Yi, Wang Jiasheng. Combined effects of cooled EGR and a higher geometric compression ratio on thermal efficiency improvement of a down-sized boosted spark-ignition directed-injection engine. Energy Convers Manage 2014;78:65–73.
[15] Chen Longhua, Li Tie, Yin Tao, Zheng Bin. A predictive model for knock onset in spark-ignition engines with cooled EGR. Energy Convers Manage 2014;87:946–55.
[16] Bechtold RL. Alternative fuels guidebool. SAE International; 1997.
[17] Heywood JB. Internal combustion engine fundamentals. McGraw-Hill; 1988.
[18] Hou S, Schmidt DP. Interaction mechanisms between closely spaced sprays. SAE Paper 2008-01-0946.
[19] Hung DLS, Zhu GG, Winkelman JR, Stuecken T, Schock H, Fedews A. A high speed flow visualization study of fuel spray pattern effect on mixture formation in a low pressure direct injection gasoline engine. SAE Paper 2007-01-1411.
[20] Mitroglou N, Nouri JM, Gavaises M, Arcoumanis. Spray structure generated by multi-hole injectors for gasoline direct-injection engines. SAE Paper 2007-01-1417.
[21] Pontoppidan M, Bella G, Rocco V. Mixture formation in SI-Engine intake systems – a simplified theoretical model with experimental verification. ASME 1996 Spring Congress.
[22] Pontoppidan M, Gaviani G, Bella G, Rocco V. Direct fuel injection – a study of injector requirements for different mixture preparation concepts. SAE Paper 970628.
[23] Pontoppidan M. Combined use of 3D-CFD simulation and direct visualization techniques to decrease the optimization procedure complexity of combustion chamber layout and engine control pre-mapping operation necessary for online engine test rig optimization. In: Internationales Symposium für Verbrennungsdiagnostik. Baden-Baden; 2002. p. 137–47.
[24] Amsden AA, O'Rourke PJ, Butler CD. KIVA II a computer program for chemical reactive flows with sprays. Los Alamos National Labs. LA-11560-MS-1989.
[25] Amsden AA, O'Rourke PJ, Butler CD. KIVA III: a KIVA program with block structured mesh for complex geometries. Los Alamos National Labs. LA-12503-MS.
[26] Alkidas Alex C. Combustion advancements in gasoline engines. Energy Convers Manage 2007;48:2751–61.
[27] Alex C, Alkidas SH, Talry. Contributors to the fuel economy advantage of DISI engines over PFI engines. SAE paper 2003-01-3105.
[28] Pontoppidan M, Demaio A, Rotondi R. Parametric study of physical requirements for successful use of a homogenous charge compression ignition (HCCI) approach in a direct injected gasoline engine.
[29] Hyvonen J, Haraldsson G, Johansson B. Operating conditions using spark assisted HCCI combustion during combustion mode transfer to SI in multi-cylinder VCR-HCCI engine. SAE paper 2005-01-0109.
[30] Porpathan E, Ramesh A, Nagalingam B. Effect of swirl on the performance and combustion of a biogas fuelled spark-ignition engine. Energy Convers Manage 2013;76:463–71.
[31] Fontana G, Galloni E. Variable valve timing for fuel economy improvement in a small spark-ignition engine. Appl Energy 2009;86:96–105.
[32] Fontana G, Galloni E. Experimental analysis of a spark-ignition engine using exhaust gas recycle at WOT operation. Appl Energy 2010;87:2187–93.
[33] Caton A Jerald. The thermodynamic characteristics of high efficiency, internal-combustion engines. Energy Convers Manage 2012;58:84–93.
[34] Ayala FA, Gerty MD, Heywood JB. Effects of combustion phasing, relative air-fuel ratio, compression ratio and load in SI engine efficiency. SAE paper 2006-01-0229; 2006.
[35] Van der Wege BA, Hahn Z, Iyer CO, Munoz RB, Yi J. Development and analysis of a spray-guided DISI combustion concept. SAE paper 2003-01-3105.